CFD analysis of jet flows ejected from different nozzles

Mustafa Atmaca[1,*], Berkay Çetin[1], Cüneyt Ezgi[2] and Ergin Kosa[3]

[1]Mechanical Engineering Department, Marmara University, Istanbul 34722, Turkey;
[2]Marine Engineering Department, Piri Reis University, Istanbul 34940, Turkey;
[3]Mechanical Engineering Department, Beykent University, Istanbul 34398, Turkey

Abstract

Nozzles are widely used to control the rate of flow, speed, direction, mass, shape and pressure of the stream in connection with many different engineering applications. This paper presents the performance predicted by a computational fluid dynamic (CFD) model, which are 3D models that utilize parametric analysis, realizable k-epsilon turbulence models and experimental measurement for a jet. Jet flows are ejected from three different slot nozzles: round-shaped nozzle, rectangular-shaped nozzle and 2D-contoured nozzle. In this numerical study, velocities of free jets have been predicted for different axial distances from the nozzle exit in the range of $0.2 \leq z/B \leq 12$ when center velocity at the nozzle exit. CFD simulation results are compared to experimental results from literature. These results are consistent with the existing experiments.

1. INTRODUCTION

Nozzles are widely used in connection with many different engineering applications, mainly to generate jets and sprays. The nozzle exit flow serves as the initial condition for the downstream flow. Experiments have been conducted with variations of nozzle exit Reynolds number by Yang *et al.* [1]. They measured developing structures of free jets by hot-wire anemometer to understand the characteristics of heat transfer in conjunction with measured jet flows. In that study, different flow characteristics have been observed depending on different nozzle shapes as in the experimental study implemented.

In most instances, flow non-uniformity and turbulence originate within the nozzle, but the nozzle contraction is generally designed to attenuate and minimize these effects [2].

The jet type flows occur in a variety of applications, especially in the industrial sector. For over a century, the theory of turbulent jets and their practical applications have attracted the specialist's attention in many research fields [3, 4].

The capability for Navier–Stokes analysis of exhaust nozzle flow fields has progressed to the point that, for simple nozzle geometries, computational fluid dynamic (CFD) accuracy for performance quantities is comparable to experimental accuracy. The CFD simulation has the advantage that a discrete point approximation to the entire flow field is available [5–8]. This makes it possible to consider using the CFD solution to investigate a number of important nozzle performance effects that would be extremely difficult to investigate experimentally.

There are relatively few experimental data sets on nozzle thrust performance that are documented in the open literature in sufficient detail to be suitable for purposes of CFD verification. In this paper, the results of an investigation into utilization of scarfed, truncated perfect nozzle for thrust vector adjustment in tactical strap-on boosters are presented.

There is less published literature involving the numerical simulation of flow in nozzles. Yu *et al.* [2] have performed Reynolds-averaged Navier–Stokes simulations to investigate the effect of nozzle geometry on the turbulence characteristics of incompressible fluid flow through nozzles at Reynolds number of approximately 50 000. Four nozzles have been considered: a baseline nozzle and three modified nozzles (extended, grooved and ringed). The flow in these nozzles has been simulated using different turbulence closure models, including Spalart–Allmaras, variants of k–ε and k–ω and the Reynolds stress model. Payri *et al.* [9] and Macian *et al.* [10] numerically investigated the effect of diesel nozzle geometry on the inception and development of cavitation. Sushma *et al.* [11] presented the results of an investigation into utilization of scarfed, truncated perfect nozzle for thrust vector adjustment in tactical strap-on boosters. The purpose of Qiang *et al.*'s [12] study is the development and validation of an internal

three-phase flow model of the abrasive water jet with the capability to predict the acceleration of solid particles and the wear of nozzle wall.

Giannadakis *et al.* [13] developed a CFD cavitation model for diesel injector nozzles based on the Eulerian–Lagrangian approach. They demonstrated that their model can identify many of the cavitation structures present in internal nozzle flows and showed that these structures are dependent on nozzle design and flow conditions.

Nozzles are widely used in many different applications of engineering, especially to generate jets. While designing the nozzles, it was aimed to achieve a low turbulence density at the nozzle outlet. Therefore, this situation has been emphasized in experimental and numerical studies especially on jets. The nozzle exit flow serves as the initial condition for the downstream flow. In most instances, flow non-uniformity and turbulence originate within the nozzle, but the nozzle contraction is generally designed to attenuate and minimize these effects. The objective of this numerical study is to explain jet flow structure ejected from different shaped slot nozzles and to validate with experimental results.

In this sudsy, it is used of model-free simulations to broaden our understanding of some of underlying mechanisms involved in the near field of jet flows originating from different nozzles. Our primary objective is to assess the influence of the nozzle shape on the subsequent evolution of the jet flows and their mixing characteristics. This facilitated by analyzing the processes involved in entrainment. Three nozzles are considered: round-shaped nozzle, rectangular-shaped nozzle and 2D-contoured nozzle.

2. GEOMETRY AND GRID STRUCTURE

Three different geometries were created for rectangular-shaped nozzle, round-shaped nozzle and 2D-contoured nozzle. General structural for the computational geometries is shown as in Figure 1. Inlet zone was created at a distance of 200 mm before the end point of nozzle exit and dimensions of 60mm × 130mm. *B* is the jet width.

In the experimental study carried out by Yang *et al.* [1], measurements were taken up to 100 mm from the nozzle exit. Therefore, the data we received in the simulations had to be taken up to 100 mm accurately. In order to obtain these data, a volume of 100 × 30 × 130 mm, shown in the Figure 1, was applied to the body of influence. The body of influence influences the mesh density of the body that it is scoped to, but it is not be a part of the model geometry nor will it be meshed.

Meshes of the same characteristics were created for three different geometries. Figure 2 shows the specific locations of mesh zones. These locations are Inlet (A), outlet (B) and nozzle walls (C) and the body-of-influence volume (D).

Table 1 shows qualities of the inflation zone and the body of influence zone. Inflation was applied to named selection that shown as C (nozzle wall) in Figure 2. Inflation qualities are maximum layers 6, growth rate: 1.1. For the body of influence, growth rate and element size are given as 1.1 and 1 mm, respectively.
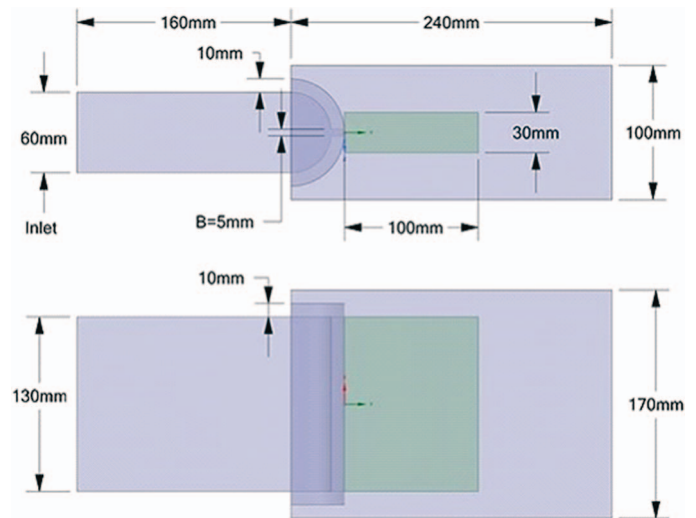

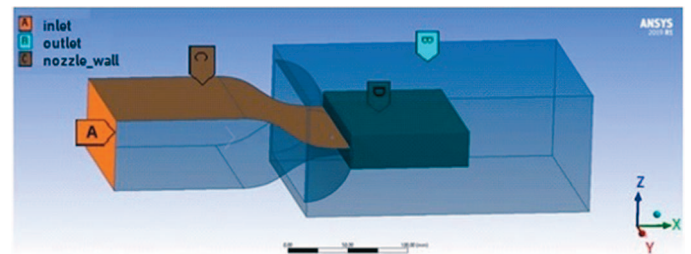**Figure 1.** *Computational geometry.*

Figure 2. *Specific locations of zones.*

Table 2 shows the mesh properties for each type of nozzles. Curvature and proximity qualities were applied for each mesh. In this study, grid independence tests were implemented to determine the optimal number of grids for each nozzle shape. Nozzles are divided into different grid numbers. 5 652 688, 6 102 688 and 5 595 724 elements were used for rectangular-shaped nozzle, round-shaped nozzle and 2D-contoured nozzle, respectively. For proximity qualities, numerical cells across gap were taken to be 6. Other mesh qualities are element size 5 mm, growth rate 1.1 and target skewness 0.8.

Grid structure is given in Figure 3 for different nozzles. When the mesh structure is examined, dense mesh was formed in the area created by body of influence. Inflation layers were formed along the nozzle walls.

2.1. Boundary conditions

Velocity inlet was defined by zone shown as A in Figure 2. The values of the velocity inlet were set as parameters. Table 3 shows input parameters and results. In order to compare the experimental results, the velocity-inlet parameter was changed and the results were approximated to the values used in the experimental results. The temperature value is given as 300 K.

Table 1. *Inflation and body sizing.*

Object name	Inflation	Object name	Body sizing
Boundary	Nozzle wall	Geometry	1 body
Inflation option	Smooth transition	Type	Body of influence
Transition ratio	0.272	Bodies of influence	1 body
Maximum layers	6	Element size	1 mm
Growth rate	1.1	Growth rate	1.1
Inflation algorithm	Pre		

Table 2. *Comparison of mesh for different nozzle types.*

Type	Rectangular-shaped nozzle	Round-shaped nozzle	2D-contoured nozzle
Nodes	7 753 126	8 461 305	7 696 092
Elements	5 652 688	6 102 688	5 595 724
Element size	5. mm	5. mm	5. mm
Growth rate	1,1	1,1	1,1
Max size	5. mm	5. mm	5 mm
Mesh defeaturing	Yes	Yes	Yes
Defeature size	2.5e-002 mm	2.5e-002 mm	2.5e-002 mm
Capture curvature	Yes	Yes	Yes
Curvature min size	5.e-002 mm	5.e-002 mm	5.e-002 mm
Curvature normal angle	18°	18°	18°
Capture proximity	Yes	Yes	Yes
Proximity min size	5.e-002 mm	5.e-002 mm	5.e-002 mm
Num cells across gap	6	6	6
Target skewness	0.8	0.8	0.8
Smoothing	High	High	High
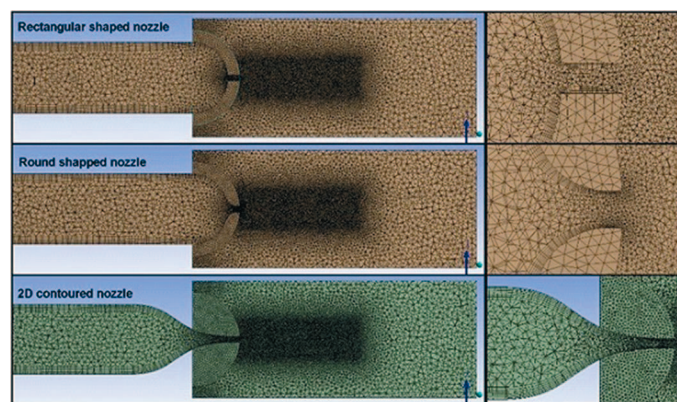
Figure 3. *Grid structure for each shape of nozzles.*

3. COMPUTATIONAL METHODS

The commercial CFD software, Fluent 19.2 [14], is utilized to compute the unsteady 3D incompressible flow. In the general setting of the CFD simulation, solver type and time are selected as pressure based and steady, respectively. In addition, the gravitational acceleration in the Y direction was magnitude of $9.81\ \mathrm{ms}^{-2}$ for simulation.

In the model setting, firstly energy equations have been activated. Then the k-epsilon model has been selected from the viscous settings and, as a wall function, realizable and standard wall functions are used in k-epsilon models.

In solution methods setting, coupled scheme is applied for pressure–velocity coupling. Coupled algorithm solves the momentum and pressure-based continuity equations together; also this algorithm improves solution convergence rate. Spatial discretization settings, least-squares-cell based and second-order are implemented for gradient and pressure-interpolation-schemes, respectively. Second-order upwind schemes are selected for momentum, turbulent kinetic energy and turbulent dissipation rate. Hybrid initialization is applied and 1000 iterations are defined, solved and converged for each simulation. Each model is converged. The convergence criteria are 10^{-6} and 10^{-8} for the flow field and energy equations, respectively.

Table 3. *Velocity input–output parameters.*

Nozzle type	Inlet velocity (parametric) m/s	Maximum value of velocity on line	
		$Y = 0.001$ m ($z/B = 0.2$) m/s	$Y = 0.005$ m ($z/B = 1$) m/s
Rectangular-shaped nozzle	2.715	40.345	39.615
Round-shaped nozzle	3.270	40.351	40.368
2D-contoured nozzle	3.200	40.061	40.078
2D-contoured nozzle	3.270	40.927	40.945

Air is used as material and its properties are default. Even if the properties of the air define as ideal gas models or real gas models, the simulations results did not change greatly. For this reason, properties of material were used by default. Properties of air that used for simulation are the following: density, ρ=1.225 kgm^{-3}; heat capacity, c_p = 1006.43 Jkg^{-1} K^{-1}; thermal conductivity, k = 0.0242 Wm^{-1} K^{-1}; viscosity, μ = 1.7894 × 10^{-5} kgm^{-1} s^{-1}.

3.1. Governing equations

In the current study, the CFD code was used for 3D numerical simulations of fluid flow. The developed model simultaneously solves the mass, momentum and energy conservation equations. Generally, for an incompressible flow, these equations are as follows [5, 8]:

$$\frac{\partial}{\partial x_j}\left(f_j \rho u_j\right) = 0 \qquad (1)$$

$$\frac{\partial}{\partial x_j}\left(f_j \rho u_i u_j\right) = -f_v\frac{\partial p}{\partial x_i} + \frac{\partial}{\partial x_j}\left(f_j \tau_{ji}\right) + R_i + f_v\rho S_{u_i} \qquad (2)$$

$$\frac{\partial}{\partial x_j}\left(f_j \rho u_i T\right) = \frac{\partial}{\partial x_j}\left(f_j \frac{k}{c_p}\frac{\partial T}{\partial x_j}\right) + f_v\frac{\varphi}{c_p} \qquad (3)$$

Turbulent kinetic energy:

$$\frac{\partial}{\partial t}\left(\rho k\right) + \frac{\partial}{\partial x_j}\left(\rho \varepsilon u_i\right) = \frac{\partial}{\partial x_j}\left(\alpha_z \mu_{eff}\frac{\partial \varepsilon}{\partial x_j}\right) + C_k + \rho\varepsilon \qquad (4)$$

Turbulent energy dissipation:

$$\frac{\partial}{\partial t}\left(\rho\varepsilon\right) + \frac{\partial}{\partial x_i}\left(\rho\varepsilon u_i\right) = \frac{\partial}{\partial x_j}\left(\alpha_z \mu_{eff}\frac{\partial \varepsilon}{\partial x_j}\right) + C'_{1z}\frac{\varepsilon}{k}G_k - C_{2z}\rho\frac{\varepsilon^2}{k} \qquad (5)$$

where

$$\mu_{eff} = \mu + \mu_t, \quad \mu_t = \rho c_\mu\frac{k^2}{\varepsilon}, \quad C'_{1z} = C_{1z} - \frac{\mu\left(1 - \mu/\mu_0\right)}{1 + \beta\eta^3} \qquad (6)$$

$$\eta = \left(2E_{ij}\cdot E_{ij}\right)^{1/2}\frac{k}{\varepsilon}, \quad E_{ij} = \frac{1}{2}\left(\frac{\partial u_i}{\partial x_j} + \frac{\partial u_j}{\partial x_i}\right) \qquad (7)$$

4. RESULTS AND DISCUSSION

CFD results are shown by the variables and values used in the experimental study by Yang et al. [1]. In the experimental study, U_j is the exit velocity of the nozzle. B is the width of the nozzle and B = 5 mm.

Figure 4 illustrates coordinates where CFD and experimental results are received. The term z/B defines the distance from the nozzle, while the term y/B defines the locations of the data line.
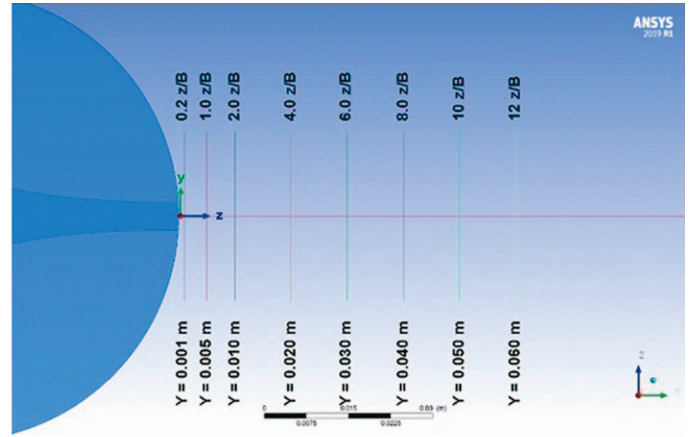

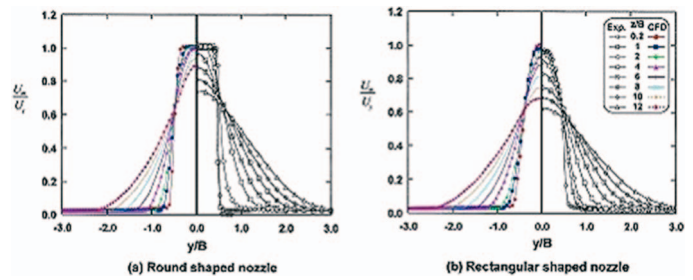**Figure 4.** *Schematic representation of the data locations.*

Figure 5. *Widthwise variations of mean velocity as experimentally and numerically for different nozzle shapes at Uj = 40 m/s: (a) round-shaped nozzle and (b) rectangular-shaped nozzle.*

In Figure 5, the velocity distributions for round-shaped nozzle and rectangular-shaped nozzle at U_j = 40 ms^{-1} are experimentally and numerically shown. As can be seen in Figure 5, it is clearly stated that experimental results presented by Yang et al. [1] and numerical results are similar. In the experimental study, the exit speed of the nozzle was taken as 40 ms^{-1}. In the CFD simulation, parametric analysis was performed for 40 ms^{-1} convergence of nozzle output speed. As a result of the parametric analysis, the appropriate inlet velocity was determined. The inlet velocity value for the rectangular-shaped nozzle shown in Table 3 was determined as 2.715 ms^{-1}. As a result of this input speed, the maximum velocity formed on the line Y = 0.001 m (z/B = 0.2) is 40.345 ms^{-1}. The inlet velocity value for the round-shaped nozzle is 3.27 ms^{-1} and the maximum velocity taken over the line Y = 0.001 m (z/B = 0.2) is 40.351 ms^{-1}. The Table 3 also shows the results of the 2D-contoured nozzle. Table 3 shows that the velocity-inlet value differs for each nozzle.

For the round-shaped nozzle, there are uniformly distributed velocities along the y/B (width), whereas for the rectangular-shaped nozzle it does not seem to be distributed so uniformly. This is clearly seen in the CFD simulation. For the round-shaped nozzle, the speed reduction at y/B = 0 (center line) is less than for the rectangular-shaped nozzle.
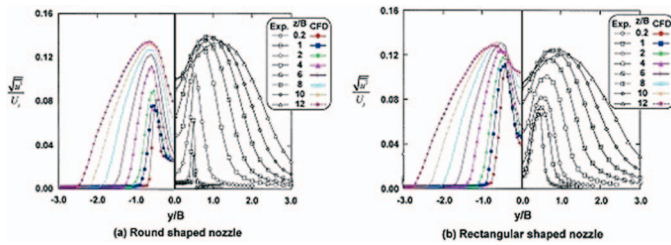
Figure 6. *Widthwise variations of velocity fluctuations as experimentally and numerically for different nozzle shapes at Uj = 40 m/s: (a) round-shaped nozzle and (b) rectangular-shaped nozzle.*

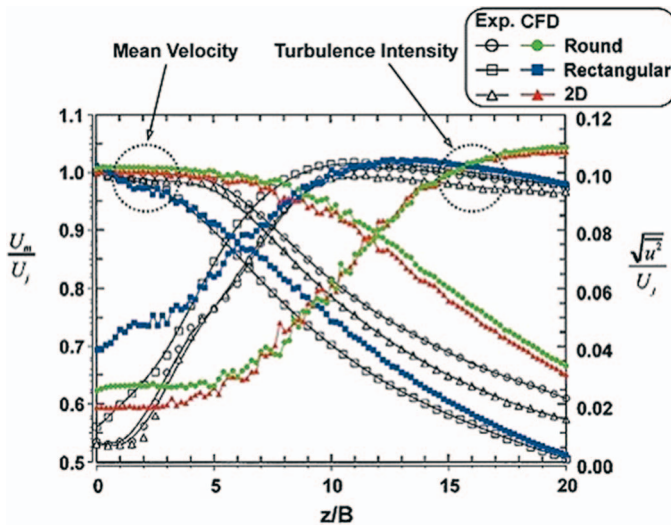
Figure 7. *Axial variations of jet flow structure for different nozzle shapes for Uj = 40 m/s.*

In Figure 6, normalized velocity fluctuations, i.e. turbulence intensities, in the widthwise direction for round-shaped nozzle and rectangular-shaped nozzle at $U_j = 40$ ms^{-1} are experimentally and numerically shown.

As shown in Figure 7, the numerical results are similar to the experimental results for all nozzle shapes, particularly at some values of z/B. The maximum turbulence intensity in the centerline for a rectangular shaped is observed experimentally and numerically at $z/B = 12$. Turbulence intensities at this point are about 9% and 10.5% experimentally and numerically, respectively. The maximum turbulence intensity in the centerline for a round shaped are 8% for numerically and 10% for experimentally.

The lowest turbulence intensity in the centerline for a rectangular shaped is observed at $z/B = 0.2$. Turbulence intensities obtained at this point experimentally and numerically are about 2% and 4%, respectively.

Figure 7 shows the axial variations of jet flows along the centerline for three different nozzles with the increase of axial distance from nozzle exit in the range of at $0 < z/B < 20$ at $U_j = 40$ ms-1as experimentally and numerically.

For round-rectangular nozzle, the experimental and numerical results were very close for all z/B values. For round-shaped nozzle and 2D-contoured nozzle, the experimental and numerical results were very close to each other at $0 \leq z/B \leq 5$ and $14 \leq z/B \leq 20$. However, at other z/B ranges, deviations have occurred.

5. CONCLUSION

Despite some differences, experimental results and numerical results gave appropriate results. These differences can be explained as follows:

In the experimental study, air passes through the blower, valve and settling chamber and the flow is made uniform and emerges from the nozzle. The equipment used in the experimental study was adjusted according to the nozzle types so that the nozzle output speed (U_j) could be 40 ms^{-1}. The flow rate of the uniform flow was varied for different nozzle types. In the CFD study, the flow is defined as uniform in the inlet region.

In addition, in the experimental study, measurements were made by taking time averages in a certain region of the experimental setup. In numerical analysis, the correct use of these measured values is not suitable for CFD algorithm. In any region, parametric analysis should be performed in accordance with the CFD algorithm to obtain the results measured by time averaging. The results found in the experimental study should be convergent in CFD.

Numerical investigations are carried out by comparing experimental results by Yang *et al.* [1] for three different nozzles. These simulations indicate that these studies can be performed easily with CFD. Numerical values are generally consistent with the experimental results. However, some deviations are observed. Also, as a result of these simulations, it has been seen that certain changes in nozzle geometry can result in major changes to the operating conditions of the nozzle, and this can have significant impact on flow characteristics.

REFERENCES

[1] Yang G, Choi M, Lee JS. An experimental study of slot jet impingement cooling on concave surface effects of nozzle configuration and curvature. *Int J Heat Mass Transf* 1999;**42**:2199–209.

[2] Yu Y, Shademan M, Barron RM *et al.* CFD study of effects of geometry variations on flow in a nozzle. *Eng Appl Comp Fluid* 2012;**6**:412–25.

[3] Abbassi A, Kechiche N, Ben Aissia H. Prandtl-number effects on vertical buoyant jets in forced and mixed convection regimes. *Energy Convers Manag* 2007;**48**:1435–49.

[4] Kriaa W, Ben Cheikh H, Mhiri H *et al.* Numerical study of free pulsed jet flow with variable density. *Energy Convers Manag* 2008;**49**:1141–55.

[5] Atmaca M, Girgin I, Ezgi C. CFD modelling of a diesel evaporator used in cell systems. *Int J Hydrog Energy* 2016;**41**:6004–12.

[6] Atmaca M, Çetin B, Yılmaz ECFD. Analysis of unmanned aerial vehicles (UAV) moving in flocks. *Acta Phys Pol A* 2019;**135**:694–6.

[7] Atmaca M. Wind tunnel experiments and CFD simulations for gable-roof buildings with different roof slopes. *Acta Phys Pol A* 2019;**135**:690–3.

[8]   Atmaca M, Ezgi C. Three-dimensional CFD modeling of a steam ejector. *Energ Source Part A* 2019;1–12.

[9]   Payri R, Garcia JM, Salvador FJ *et al.* Using spray momentum flux measurements to understand the influence of diesel nozzle geometry on spray characteristics. *Fuel* 2005;**84**:551–61.

[10] Macian V, Payri R, Margot X *et al.* A CFD analysis of the influence of nozzle geometry on the inception of cavitation. *At Sprays* 2003;**13**: 579–604.

[11] Sushma L, Deepik AU, Sunnam SK *et al.* CFD investigation for different nozzle jets. *Mater Today* 2017;**4**:9087–94.

[12] Qiang Z, Wu M, Miao X *et al.* CFD research on particle movement and nozzle wear in the abrasive water jet cutting head. *Int J Adv Manuf Tech* 2018;**95**:4091–100.

[13] Giannadakis E, Gavaises M, Arcoumanis C. Modelling of cavitation in diesel injector nozzles. *J Fluid Mech* 2008;**616**:153–93.

[14] ANSYS FLUENT user's guide. 2018. FLUENT Inc.